

Iron Powder Treated Gray Irons: Critical Shape Characteristics for Graphite Nuclei

Stelian Stan, Mihai Chisamera, Iulian Riposan, Nicoleta Ivan, and Michael Barstow

(Submitted March 15, 2011; in revised form October 3, 2011)

A program was conducted to research how to characterize the size and shape of micro-particles. These can act as graphite nuclei, but are altered by adding a commercial iron powder, or after a similar treatment combined with inoculation. Resin sand mold (RSM) and metal mold (MM) solidified sample structures were subjected to automatic image analysis. In general, a higher cooling rate, typical for MM solidification, favors smaller size and more compact particles, even in RSM media. Iron powder treatment led to the largest particles with unusual morphologies, better defined by complex shape factors, which employ actual perimeters, rather than the simpler median size and aspect ratio method. Conventional inoculation employed after an iron powder treatment altered the particles (smaller and more compact), which benefited their effectiveness to act as graphite nuclei, especially at slower solidification rates in RSMs. The results confirm that promoting more compact micro-inclusions, at smaller sizes, involved in graphite nucleation, reduces the sensitivity to chill and improves the eutectic cell characteristics in gray cast iron.

Keywords chill, eutectic cell, graphite nuclei, gray iron, inoculation, iron powder, morphology, shape factors

1. Introduction

Gray cast irons characteristically excel in many physical properties such as machinability, heat conductivity, and vibration damping capacity. These important properties, in combination with reasonable strength, contribute to gray iron being the primary choice, usually with hypoeutectic chemistries, in the production of essential vehicle engine components.

Eutectic to slightly hypereutectic compositions (carbon equivalent CE = 4.3–4.5 wt.%) provide the best combination of castability, tensile strength, and thermal properties, especially for thin wall gray iron castings. Commercial cast iron is a typical eutectic alloy. Eutectic reaction under non-equilibrium cooling is a key aspect of non-equilibrium solidification, with quasi-eutectic formation of this iron, as a direct result of undercooling and the concept of a coexisting region.

Thus, the structure developed during non-equilibrium solidification is far more complicated than that under equilibrium conditions (Ref 1, 2). Eutectic solidification starts with the independent nucleation of austenite and graphite from the melt. Austenite grows dendritically. Dendritic growth of austenite continues until austenite dendrites contact each other, defining the grain structure (Ref 3–5).

The amount and length of austenite dendrites play a significant but neglected role in the strength of cast iron. The greater the dendrite amount, the stronger the cast iron is. Larger

quantities of primary austenite dendrites increase tensile strength by reinforcing the matrix, similar to fibers in a composite, and can be produced in several ways: by iron melt superheating, reducing the carbon equivalent, providing materials to serve as substrates for austenite nucleation, adding elements which promote undercooling, increasing the cooling rate, and inoculation with specific elements (Ref 6–8).

As the carbon equivalent (CE) increases, the amount of austenite dendrites decreases. But, due to non equilibrium solidification, a complex structure with eutectic cells “reinforced” by austenite dendrites can be obtained in eutectic and hypereutectic gray cast irons (CE = 4.3–4.5%), more evident at higher eutectic undercooling, providing an opportunity to improve their mechanical properties (Ref 9).

A 0.1–1.0 wt.% addition of pure iron powder in hypoeutectic gray irons (CE = 3.7–4.3%) appears to have an interesting influence on the formation of austenite dendrites and their characteristics. Notably, pure iron has the same crystal structure as the primary phase of the solidifying metal. It was confirmed that the largest effect on primary dendrites is achieved by a treatment involving pure iron powder (Ref 10–12).

Iron powder additions in eutectic to slightly hypereutectic gray irons were also important to promote austenite dendrites, but with some accompanying negative effects on chill tendency and eutectic cell characteristics. However, supplementary “conventional” inoculation, in a double treatment, appears to preserve some of the desirable effects on both austenite and eutectic cell formation. Figure 1, derived from already published data (Ref 13, 14) summarizes the unusual effects of the different treatments, including iron powder and/or inoculation in these irons. An earlier simple characterization of the graphite nuclei morphology as median size and maximum to minimum size ratio (aspect ratio as a simple shape factor) led to a better understanding of the effects of each treatment, but had limited ability to explain these phenomena (Ref 13–15).

Electron microscopy has revealed the nucleus for a graphite flake consists of a particle, usually less than 6 μm in size, with

Stelian Stan, Mihai Chisamera, Iulian Riposan, and Nicoleta Ivan, POLITEHNICA University of Bucharest, 313 Spl. Independentei, 060042 Bucharest, Romania; and Michael Barstow, Consultant Metallurgist, Fremont, CA. Contact e-mail: riposan@foundry.pub.ro.

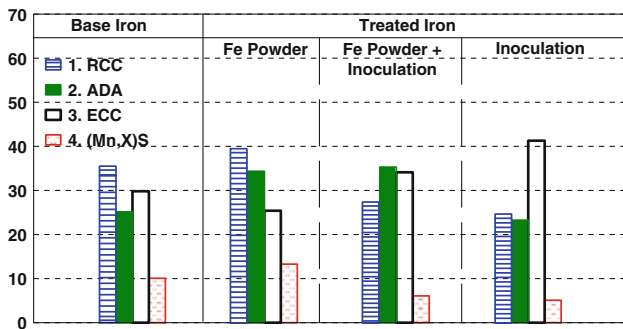


Fig. 1 Average relative clear chill (RCC, %, W_1 , RSM), austenite dendrite area (ADA, %, MM), eutectic cell count (ECC, cm^{-1} , RSM), and (Mn,X)S compounds size (μm , RSM) in irons solidified in RSM and MM

a body of sulfide [(Mn,X)S type] around a nucleus core of complex oxide (usually less than $2 \mu\text{m}$ size) (Ref 16-20). The nucleation of graphite on MnS particles was also confirmed by microstructure simulation (Ref 21-23).

The main objective of the present study is to conduct a more complete characterization of micro-particles [(Mn,X)S type], which participate within nuclei of graphite in iron powder treated, slightly hypereutectic gray irons, either alone or in a double treatment with Ca,Ba,Al-FeSi inoculation. The characterization was based on size distribution and complex shape factors, and was then related to their role in controlling chill (carbides) formation and how they affected the characteristics of the eutectic. The more a particle deviates from an ideal shape such as a sphere, the more difficult it is to agree on a set of parameters, which might define the irregular shape. Some of the particles under consideration in this program are described as like Chinese script, which is a subjective comment suggesting highly intricate outlines. Since previous research had demonstrated that iron powder additions transformed some of these (Mn,X)S particles into larger, more irregular, less dense morphologies it is of significant interest to this study to determine the different shapes quantitatively. The principal emphasis of this exercise therefore was to consider the different ways a particles irregularity could be accurately defined. The various descriptions of “sphericity” or “elongation” or “circularity” are an attempt to distinguish levels of “roundness” by employing combinations of area and perimeter length, either actual or approximated (smoothed).

2. Experimental Procedure

The experimental heat was produced in an induction furnace (acid lining, 100 kg, 2400 Hz). The iron melt was heated to $1530 \text{ }^\circ\text{C}$ for 5 min, then tapped at $1500 \text{ }^\circ\text{C}$ into a pouring ladle (10 kg iron) and a treatment ladle (25 kg iron), with a 1.0 wt.% Fe powder addition during tap.

The iron powder used had the following chemistry (maximum wt.%: 0.02C, 0.05Si, 0.2Mn, 0.015P, 0.015S, 0.3O₂, Fe-bal) and characteristics (0.4-1.0 mm particle size, 2.7-3.0 g cm^{-3} apparent density). A proprietary FeSi inoculant, containing Ca, Ba, and Al (wt.%: 0.75-1.25Ca, 0.75-1.25Ba, 0.75-1.25Al, 73-78Si, Fe-bal and 0.2-0.7 mm particle size),

was added at 0.2 wt.% after the iron powder, in a double treatment. Test bars at 25 mm diameter in resin sand molds (RSMs) and 30 mm in metal mold (MMs), were cast at $1340 \text{ }^\circ\text{C}$. A final chemistry in a slightly hypereutectic range was maintained in the following ranges: 4.35-4.45%CE, 3.62-3.70%C, 2.19-2.34%Si, 0.47-0.48%Mn, 0.032-0.040%S, and 0.15%P. Other residual elements were kept at negligible levels.

Structure analysis was performed using an Automatic Image Analyzer [analySIS[®] FIVE Digital Imaging Solutions software], with the focus on the characteristics of micro-particles of the MnS type, which have been found to act as substrates for nucleation sites of flake graphite. 13-17 representative micro-particles were selected for each test iron. The following technique was applied: (a) metallographic identification at 1000:1 on the aspect (morphology) of each selected particle; (b) measurement of representative geometric parameters for each particle [A , P_r , P_c , D (min/mean/max), Feret (min/mean/max), a , b]; (c) calculus on the representative sizes and parameters affecting the morphology (AR , E , F_s , F_c) (Fig. 2).

3. Results and Discussion

Figure 3 shows the typical morphologies of analyzed microparticles, in the (Mn,X)S system, which acted as nuclei of graphite in untreated iron and two treated irons, solidified in RSMs and MMs, respectively (Ref 14). Tables 1 and 2 illustrate the results defining the characteristics in terms of size and morphology.

A large variation in the size and morphological parameters of these particles was observed, depending on the cooling rate due to the differing thermal characteristics of the molds and also the treatments applied to the molten iron. It was confirmed that the characteristics of the micro-particles depended on the cooling rate with smaller size and higher compactness at higher cooling rate, typical of MM solidification (Ref 17-20).

The characteristics as aspect, size and morphologies of the micro-particles, found to act as graphite nucleation sites in base (untreated) iron, visibly depend on the solidification rate (Fig. 4-7). In general, iron solidified in RSMs display larger micro-particles, up to twice the area and size, compared to MM. On the other hand, micro-particles in base iron solidified in MMs have lower specific perimeters and aspect ratios, so their compactness is also up to 40% higher, compared to RSM samples.

Iron powder additions appear to have the most important influence, as this treatment led to noticeable transformation of the (Mn,X)S particles from all standpoints, including a dependency on the solidification rate of the irons (see Fig. 3).

For slower cooling rates, typical for RSMs, all of the particle characteristics are at the highest levels: the largest particles (more than two times larger compared to the base iron), not just at the highest size (area) but also with the longest perimeter, especially as a real perimeter (P_r) measure; the least compactness, measured as a circularity shape factor (F_c).

The degree of compactness of micro-inclusions in iron powder treated irons appears to be less as defined by the circularity shape factor (F_c) compared to the sphericity shape factor (F_s), especially for slower solidification rates, found in RSMs (Fig. 7). The F_c shape factor is a function of the real perimeter and the area of the analyzed particle, with a larger

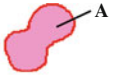
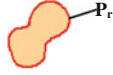
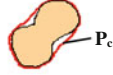
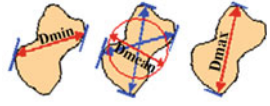
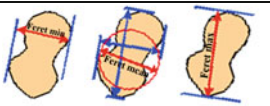
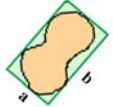
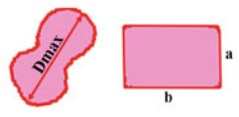
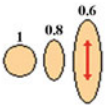
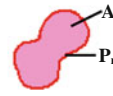
No	Parameter	2D-Geometrical features	Definition
1	Area (A)		The area of the measured particles.
2	Real perimeter (P _r)		The sum of the pixel distances along the closed boundary.
3	Convex perimeter (P _c)		The perimeter of the convex cover of the measured particle.
4	Diameter min/mean/max (D _{min} /mean/max)		The minimum/mean/maximum diameter of the measured particles (for angles in the range of 0° through 179° with step 1°).
5	Feret min/mean/max		The minimum/mean/maximum distance of parallel tangents at opposing measured particle borders.
6	Aspect ratio [AR = b/a] AR > 1		The maximum ratio of height (b) and width (a) of a rectangular boundary for the measured particle.
7	Elongation (E) [E = D _{max} /a] E > 1		The ratio of the maximum diameter (D _{max}) and the equivalent rectangle shortest side (a) (the rectangle which has the same area and perimeter as the particle).
8	Sphericity (F _s) (roundness) F _s ≤ 1		Describes the spheroidal shape or „roundness” by using the central moments, $\mu_{p,q}$ $\mu_{p,q} = \iint (x - x_c)^p (y - y_c)^q f(x,y) dx dy$ <p>p,q – central moment indices x_c,y_c – center of gravity coordinates</p>
9	Circularity (F _c) (shape factor) [F _c = 4.π.A/P _r ²] F _c ≤ 1		Provides information about the particle „roundness” by using the area (A) and the real perimeter (P _r) of the measured particle.

Fig. 2 Parameters of analyzed micro-particles

contribution from the perimeter. The factor for a circle is 1.0 and much less for different objects.

The unusual morphology of the particles found in iron powder treated iron, like “Chinese script” or a “starfish” footprint led to the least compact particles. In previous experiments, this complex sulfide morphology has less ability to nucleate graphite, leading to the formation of type D graphite (Ref 20).

Conventional inoculation with a Ca, Ba, Al-FeSi alloy after an iron powder treatment has a strong enough effect to restore more favorable characteristics of the micro-inclusions, for both cooling rates, but more so for solidification in RSMs. The size of these particles was up to three times less than those in iron

powder treated iron and 10-15% smaller than those in the base iron.

The greatest degree of particle compaction was observed in the double treated irons, almost without influence by the solidification rate (RSM and MM samples), with reference to each of the shape factors (aspect ratio, elongation, sphericity, circularity) (Fig. 6, 7). The conversion to more compact micro-inclusions by incorporating conventional inoculation after iron powder treatment is revealed more by using actual perimeter within a shape factor, such as circularity (F_c).

In previous experiments (Ref 16-20) it was determined that not only the chemistry but also the physical characteristics of (Mn,X)S compounds influence their ability to nucleate graph-

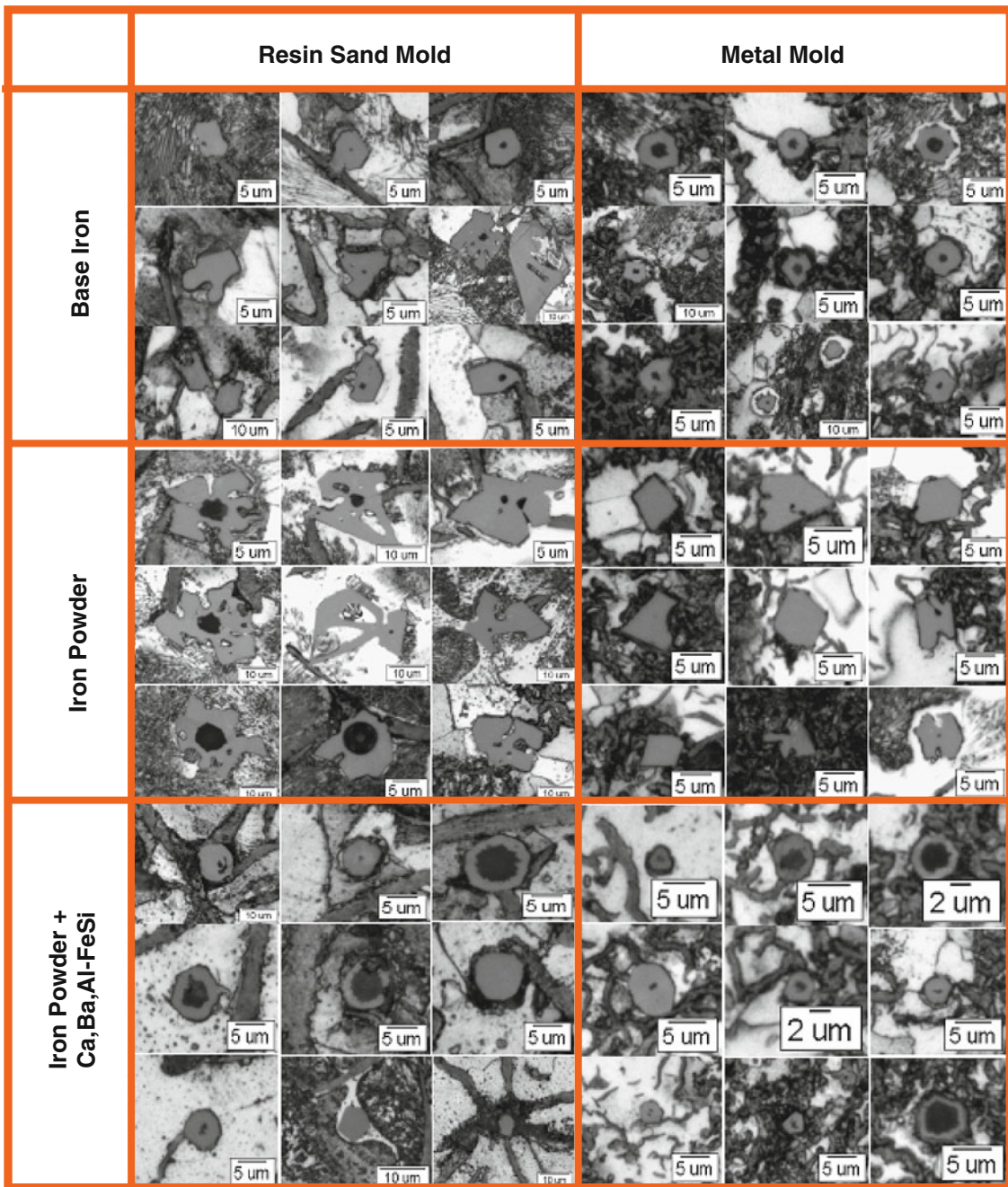


Fig. 3 Typical morphologies of analyzed micro-particles

ite. Generally smaller, more compact (Mn,X)S particles are more likely to become nucleation sites for graphite in gray cast irons. More effective nuclei reduce eutectic undercooling resulting in fewer carbides and/or a higher count of smaller sized eutectic cells with type A graphite, which describes a preferred eutectic structure.

Figure 8 illustrates the influence of the circularity shape factor (F_c) of MnS type particles in samples solidified in RSMS and MMs, on the relative total chill (RTC) and eutectic cell count (ECC) in slightly hypereutectic gray irons, (reported previously) (Ref 15).

The chill sensitivity of cast irons (carbides) decreased when the micro-particles, which participate in graphite nuclei in these irons, became more compact (Fig. 8a). This is true for both RSM and MM solidification.

In castings produced in RSMS, this influence is greater for thin wall castings, represented here by the W_1 wedge sample ($B = 5.1$ mm maximum width and $CM = 0.11$ cm cooling modulus), compared to a medium cooling rate (W_2 wedge, $B = 10.2$ mm, $CM = 0.21$ cm) and larger castings, represented by a W_3 wedge ($B = 19.1$ mm, $CM = 0.35$ cm), according to ASTM A 367.

Table 1 Measured parameters

Iron	Mold type	Area (A), μm^2	Perimeter, μm		Diameter, μm			Feret mean, μm
			Real (P_r)	Convex (P_c)	Minimum	Maximum	Mean	
Base iron	Resin sand	25.9-54.9 [37.2]	21.4-38.2 [29.1]	20.5-32.8 [25.5]	4.9-9.3 [6.4]	7.2-11.5 [9.1]	6.5-10.4 [8.2]	6.7-10.1 [7.9]
	Metal	7.6-30.7 [18.9]	11.5-21.4 [17.3]	11.3-20.9 [16.7]	3.2-6.1 [4.7]	4.1-6.9 [5.7]	3.6-6.6 [5.3]	3.6-6.6 [5.2]
Fe powder	Resin sand	110.6-345.4 [200.6]	43.2-165.8 [91.9]	43.3-87.3 [64.9]	10.0-23.7 [16.7]	13.9-30.4 [22.7]	13.5-27.5 [20.6]	13.2-26.4 [19.7]
	Metal	19.9-52.7 [36.1]	17.6-31.7 [25.9]	18.1-28.6 [24.4]	4.7-7.5 [6.4]	6.2-10.1 [8.5]	5.8-9.2 [7.9]	5.6-8.8 [7.6]
Fe powder + inoculant	Resin sand	15.0-97.2 [39.7]	17.1-37.2 [24.0]	14.8-33.7 [23.3]	3.7-9.9 [6.5]	5.1-12.3 [7.7]	4.6-11.7 [7.2]	4.6-11.6 [6.5]
	Metal	4.4-31.2 [13.7]	9.0-20.4 [13.1]	9.2-21.1 [13.3]	2.2-5.4 [3.8]	2.7-7.4 [4.5]	2.5-6.7 [4.2]	2.5-6.6 [4.2]

[...] Average value

Table 2 Shape factors

Iron	Mold type	Aspect ratio (AR)	Elongation (E)	Sphericity (F_s)	Circularity (F_c)
Base iron	Resin sand	1.06-1.89 [1.41]	1.02-1.78 [1.39]	0.32-0.96 [0.56]	0.34-0.82 [0.58]
	Metal	1.10-1.51 [1.19]	1.07-1.48 [1.15]	0.46-0.88 [0.78]	0.61-0.91 [0.78]
Fe powder	Resin sand	1.07-2.06 [1.37]	1.06-2.47 [1.46]	0.16-0.89 [0.53]	0.11-0.84 [0.37]
	Metal	1.09-1.48 [1.27]	1.03-1.40 [1.22]	0.51-0.94 [0.69]	0.31-0.86 [0.69]
Fe powder + inoculant	Resin sand	1.04-1.35 [1.16]	1.02-1.36 [1.14]	0.54-0.87 [0.78]	0.53-0.94 [0.81]
	Metal	1.05-1.31 [1.16]	1.02-1.32 [1.14]	0.57-0.96 [0.79]	0.88-0.95 [0.91]

[...] Average value

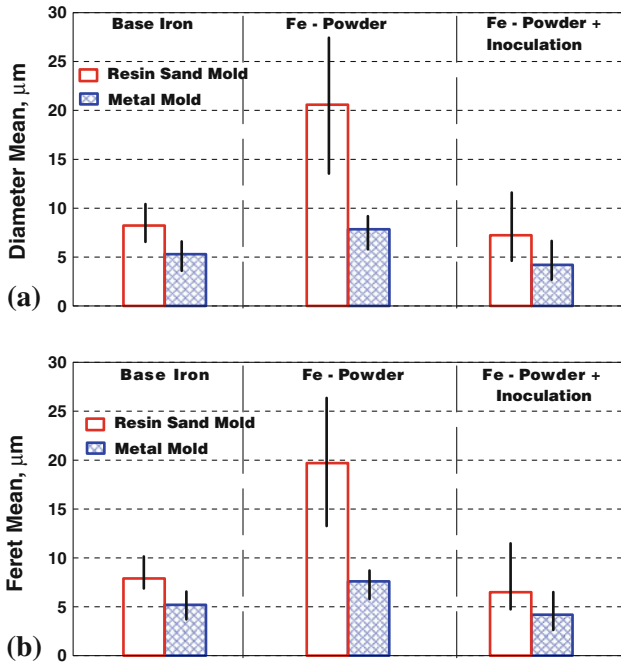


Fig. 4 Diameter mean (a) and Feret mean (b) of micro-particles in base iron and treated irons solidified in RSMs and MMs

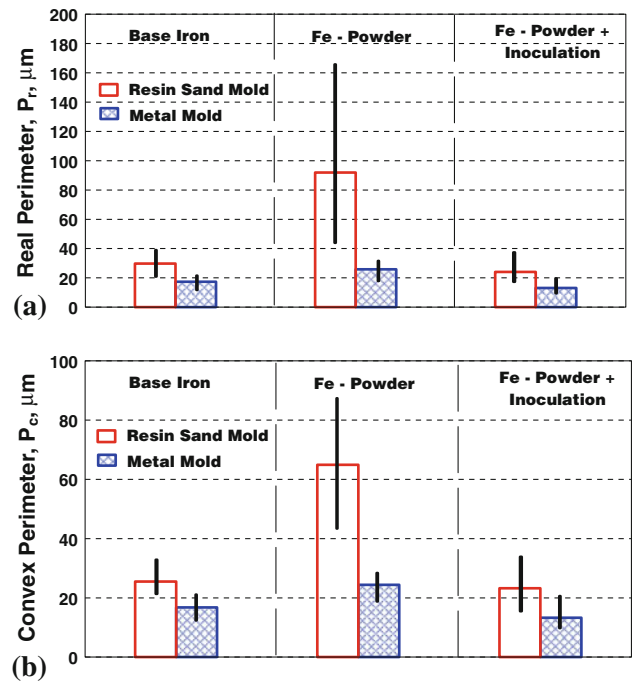


Fig. 5 Real perimeter (P_r) (a) and convex perimeter (P_c) (b) of micro-particles in base iron and treated irons solidified in RSMs and MMs

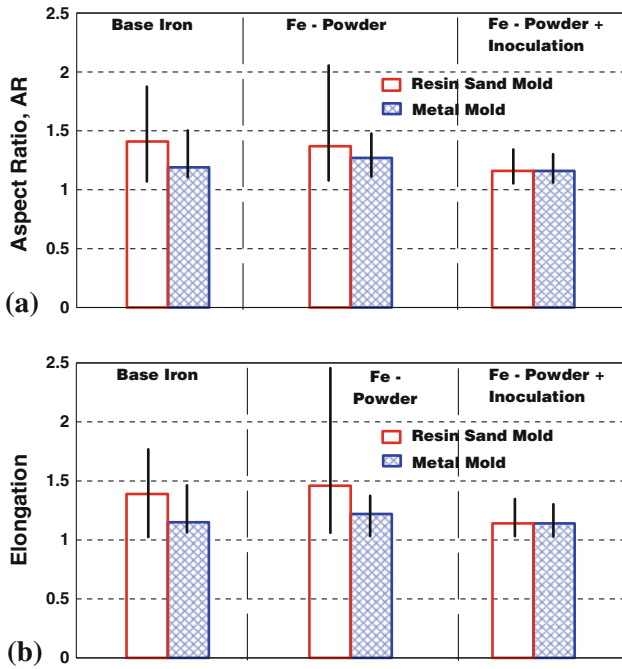


Fig. 6 Aspect ratio AR (a) and elongation E (b) of micro-particles in base iron and treated irons solidified in RSMs and MMs

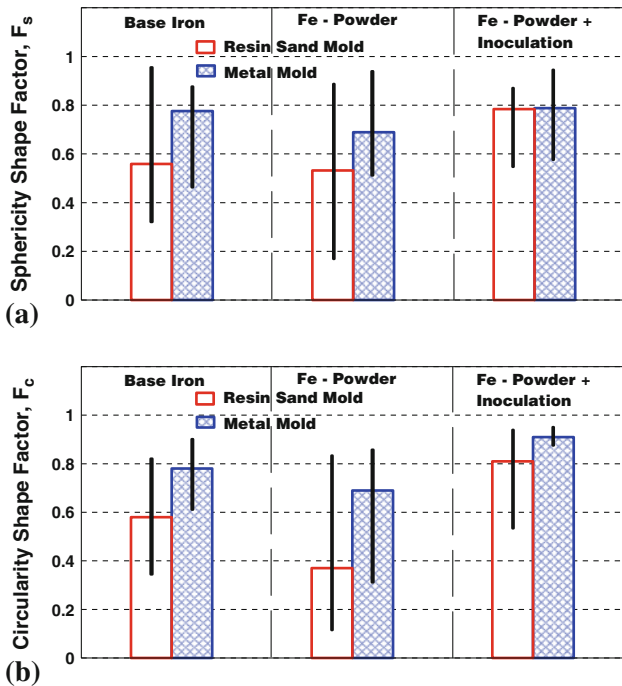


Fig. 7 Sphericity F_s (a) and circularity F_c (b) shape factors of micro-particles in base iron and treated irons solidified in RSMs and MMs

The RTC is defined by Eq 1 (Ref 24):

$$RTC = 100[W_t/B], \quad \% \quad (\text{Eq 1})$$

where B is the maximum width of the test wedge, while W_t is the width of the region from the junction of gray fracture to the first appearance of chilled iron (white spots).

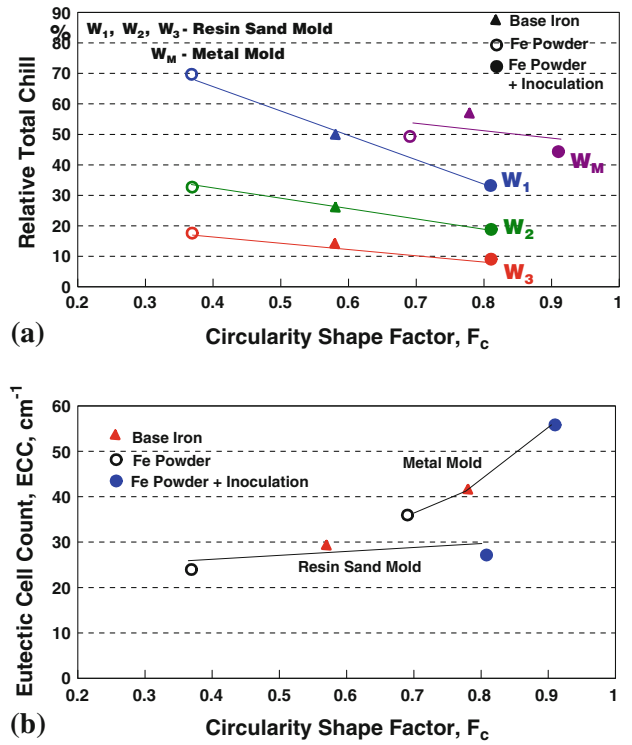


Fig. 8 Influence of the circularity shape factor (F_c) of (Mn,X)S within graphite nuclei on RTC (a) and ECC (b) of test irons (W , wedge samples)

The eutectic cell parameters show a similar progression, with decreasing size accompanied by an increasing count (Fig. 8b). Eutectic cells were characterized at mid radius on 25 mm diameter samples cast in RSMs and 30 mm diameter in MMs.

4. Conclusions

- The parameters describing the size and morphology of micro-inclusions, which can ultimately act as nucleation sites for flake graphite in slightly hypereutectic gray cast irons, depend on the applied treatment and solidification rate.
- Generally, higher cooling rates typical for MM solidification, favor smaller more compact particles, even in thin sections in RSMs.
- Iron powder treatment led to the largest particles with unusual morphologies. These effects are more apparent if characterized by complex shape factors involving the actual perimeter, rather than the original simpler approach using median size and aspect ratio.
- Using conventional inoculation after an iron powder treatment restored more suitable characteristics of MnS type particles (smaller and more compact), especially at slower solidification rates in RSM samples.
- It was confirmed that more compact micro-inclusions, at their smaller size, made them more active in graphite nucleation, lowering the iron's chill sensitivity with improved eutectic cell characteristics.

References

1. J. Zhou, Colour Metallography of Cast Iron, *China Foundry*, 2009, **6**(1), p 57–69
2. J. Zhou, Colour Metallography of Cast Iron, *China Foundry*, 2009, **6**(3), p 255–267
3. G. Rivera, P.R. Calvillo, R. Boeri, Y. Houbaert, and J. Sikora, Examination of the Solidification Macrostructure of Spheroidal and Flake Graphite Cast Irons Using DAAS and ESDD, *Mater. Charact.*, 2008, **59**, p 1342–1348
4. G. Rivera, R. Boeri, and J. Sikora, Influence of the Inoculation Process, the Chemical Composition and the Cooling Rate, on the Solidification Macro and Microstructure of Ductile Iron, *Int. J. Cast Met. Res.*, 2003, **16**(1–3), p 23–28
5. G. Rivera, R. Boeri, and J. Sikora, Researches Advances in Ductile Iron Solidification, *AFS Trans.*, 2003, **111**, p 979–989
6. G.F. Ruff and J.F. Wallace, Effects of Solidification Structure on the Tensile Properties of Gray Iron, *AFS Trans.*, 1978, **86**, p 23–46
7. G.X. Sun, X.M. Zhu, and H. Yan, The Effect of Inoculant on the Structure and Properties of Gray Iron, *Int. J. Cast. Met. Res.*, 1999, **11**(5), p 363–367
8. H. Miyake and A. Okada, Nucleation and Growth of Primary Austenite in Hypoeutectic Cast Irons, *AFS Trans.*, 1998, **106**, p 581–587
9. M. Chisamera, I. Riposan, S. Stan, C. Militaru, I. Anton, and M. Barstow, Inoculated Slightly Hypereutectic Gray Cast Irons, *J. Mater. Eng. Perform.*, doi:10.1007/s11665-011-9907-2, On-line First, 30 March 2011
10. A. Dioszegi, K.Z. Liu, and I.L. Svensson, Inoculation of Primary Austenite in Grey Cast Iron, *Int. J. Cast. Met. Res.*, 2007, **20**(2), p 68–72
11. L. Elmquist and A. Dioszegi, Research Report 2008:1 (ISSN 1404-0018), Jonkoping University, Sweden
12. L. Elmquist, S. Salera, and A. Dioszegi, Inoculation and its Effect on Primary Solidification Structure of Hypoeutectic Grey Cast Iron, *Int. J. Cast. Met. Res.*, 2010, **23**(2), p 124–129
13. I. Riposan, M. Chisamera, S. Stan, and M. Barstow, Influence of Iron Powder Addition on the Solidification and Structure of Slightly Hypereutectic Gray Cast Iron, *AFS Trans.*, 2011, **119**, p 389–406
14. M. Chisamera, I. Riposan, S. Stan, and M. Barstow, Structure Characteristics of Iron Powder Treated Slightly Hypereutectic Grey Irons, *Int. J. Cast. Met. Res.*, 2011, **24**(6), p 370–377
15. M. Chisamera, I. Riposan, S. Stan, C. Militaru, I. Anton, and M. Barstow, Effects of Iron Powder Addition on the Solidification Behaviour and Structure Characteristics of Hypereutectic Grey Cast Iron, *9th Int. Conf. on "Science and Processing of Cast Iron (SPCI-9)"*, November 2010 (Luxor, Egypt), CMRDI. *Key Engineering Materials-KEM*, 2011, Vol 457 [Science and Processing of Cast Iron IX], Trans. Techn. Publications, p 90–101
16. I. Riposan, M. Chisamera, S. Stan, T. Skaland, and M.I. Onsoien, Analyses of Possible Nucleation Sites in Ca/Sr Over Inoculated Gray Irons, *AFS Trans.*, 2001, **109**, p 1151–1162
17. I. Riposan, M. Chisamera, S. Stan, and T. Skaland, Graphite Nucleants (Microinclusions) Characterization in Ca/Sr Inoculated Grey Irons, *Int. J. Cast. Met. Res.*, 2003, **16**(1–3), p 105–111
18. I. Riposan, M. Chisamera, S. Stan, and T. Skaland, A New Approach on the Graphite Nucleation Mechanism in Grey Irons, *Proceedings of the AFS Cast Iron Inoculation Conference*, September 29–30, 2005 (Schaumburg, USA), p 31–41
19. M. Chisamera, I. Riposan, S. Stan, D. White, and G. Grasmø, Graphite Nucleation Control in Grey Cast Iron, *Int. J. Cast Met. Res.*, 2008, **21**(1–4), p 39–44
20. I. Riposan, M. Chisamera, S. Stan, C. Hartung, and D. White, Three-Stage Model for the Nucleation of Graphite in Grey Cast Iron, *Mater. Sci. Technol.*, 2010, **26**(12), p 1439–1447
21. A. Sommerfeld, B. Bottger, and B. Tonn, Graphite Nucleation in Cast Iron Melts Based on Solidification Experiments and Microstructure Simulation, *J. Mater. Sci. Technol.*, 2008, **24**(3), p 321–324
22. A. Sommerfeld and B. Tonn, Nucleation of Graphite in Cast Iron Melts Depending on Manganese, Sulphur and Oxygen, *Int. J. Cast Met. Res.*, 2008, **21**(1–4), p 23–26
23. A. Sommerfeld and B. Tonn, Theory of Graphite Nucleation in Lamellar Graphite Cast Iron, *Int. J. Metalcast.*, 2009, **3**(4), p 39–47
24. S. Stan, M. Chisamera, I. Riposan, E. Stefan, and M. Barstow, Solidification Pattern of Un-Inoculated and Inoculated Gray Cast Irons in Wedge Test Samples, *AFS Trans.*, 2010, **118**, p 295–309